Preprint
UCRL-JC-146024

Gas Pressure Forming of Titanium Alloys and Composites by Transformation Superplasticity

M. Frary, C. Schuh, D. C. Dunand

This article was submitted to
2001 Fall Meeting of the American Society for Metals International Symposium on Superplasticity and Superplastic Forming, Indianapolis, IN, November 4-8, 2001

U.S. Department of Energy

Lawrence Livermore National Laboratory

October 23, 2001

This work was performed under the auspices of the United States Department of Energy by the University of California, Lawrence Livermore National Laboratory under contract No. W-7405-Eng-48.

Gas Pressure Forming of Titanium Alloys and Composites by Transformation Superplasticity

Megan Frary[1,2], Christopher Schuh[1,3], David C. Dunand[1]

[1] Department of Materials Science and Engineering, Northwestern University, Evanston, IL
[2] Advanced Materials Technology, Caterpillar, Inc., Peoria, IL
[3] Materials Science and Technology Division, Lawrence Livermore National Laboratory, Livermore, CA

Abstract

By thermally cycling through their transformation temperature range, coarse-grained, polymorphic materials can be deformed superplastically, owing to the emergence of transformation mismatch plasticity (or transformation superplasticity) as a deformation mechanism. This mechanism is investigated under biaxial stress conditions during thermal cycling of unalloyed titanium, Ti-6Al-4V, and their composites (Ti/10 vol.% TiC_p, Ti-6Al-4V/10 vol% TiC_p and Ti-6Al-4V/5 vol.% TiB_w). During gas-pressure dome bulging experiments, the dome height was measured as a function of forming time. Adapting existing models of biaxial doming to the case of transformation superplasticity where the strain-rate sensitivity is unity, we verify the operation of this deformation mechanism in all experimental materials, and compare the biaxial results to uniaxial thermal cycling results on the same materials. Finally, existing thickness distribution models are compared with experimentally measured profiles.

Introduction

Titanium alloys and titanium matrix composites are useful materials in aerospace applications due to their high strength and stiffness, good corrosion resistance and low density [1]. Although titanium matrix composites typically exhibit low tensile ductility, they can be made superplastic by repeatedly cycling through their α/β transformation temperature range while applying an external stress [2]. Polymorphic thermal cycling causes internal strain in these materials, due to the volume change associated with the transformation, $\Delta V/V$, and the mismatch in the strengths and stiffnesses of each phase. Upon heating through the transformation range, the weaker polymorphic phase undergoes plastic flow (i.e., by creep at high homologous temperatures) to accommodate these transformation mismatch strains. In the absence of applied stress, the strain of transformation is generally reversible upon cooling through the transformation range. However, if a small external biasing stress is applied, deformation occurs preferentially in the direction of the applied stress during each transformation. The strain increment developed after a full thermal cycle (i.e., two transformations) has been found proportional to the applied stress [3], indicating that the average deformation is Newtonian (i.e., the stress exponent is unity on average). This type of deformation is known as transformation-mismatch plasticity, or when large strains are accumulated upon repeated cycling, transformation superplasticity. Greenwood and Johnson [3] developed a continuum-mechanics model of transformation superplasticity that predicts this linear relationship between the strain increment $\Delta\varepsilon$ after one thermal cycle and the external biasing stress, σ:

$$\Delta\varepsilon = \frac{4}{3}\frac{\Delta V}{V}\frac{5n}{4n+1}\frac{\sigma}{\sigma_i} \qquad (1)$$

where σ_i is the internal stress due to transformation and n is the creep stress exponent of the weaker phase.

The model of Greenwood and Johnson [3] assumes an isothermal transformation, which is not typically observed in two-phase alloys such as Ti-6Al-4V. Schuh and Dunand [4] studied the temperature- and time- dependencies of transformation superplasticity in Ti-6Al-4V by varying the amplitude and frequency of the thermal cycles, and they examined how a partial phase transformation affects the transformation superplasticity strain rate. These authors developed a more complex model to describe non-isothermal transformations, but established that Greenwood and Johnson's [3] isothermal model (Eq. (1)) can be used as a fair approximation.

Most research on transformation superplasticity has focused on uniaxial deformation of iron and steels [3,5-10], titanium [3,11-13,22,23], titanium alloys [11, 12, 14], zirconium [3, 13, 15], zirconium alloys [16, 17], cobalt [3,18] and uranium [3, 19, 20]. Recently, the linear dependence of Eq. (1) has been also observed under uniaxial conditions in intermetallics (e.g. Super α_2 Ti_3Al [21]), metal-matrix composites (e.g. Ti/TiC_p [22,

23], Ti-6Al-4V/TiC_p [24], Ti-6Al-4V/TiB_w [25]), and ceramics (Bi_2O_3 [26, 27]). Deformation under a multiaxial stress state can also be enhanced by transformation superplasticity. For example, more rapid powder densification can be achieved by thermal cycling about the phase transformation during hot pressing, as shown for powders of white cast iron [28], and titanium [29]. Foaming of porous titanium containing pressurized pores can also be enhanced with transformation superplasticity [30, 31]. One final example of transformation superplasticity using multiaxial stress is gas pressure forming of a thin disk clamped around its periphery, which is also the focus of the present study. Unlike the previous examples, free-bulging involves a well-characterized stress state and represents a standard for the study of multiaxial superplasticity, as well as a typical proof-of-concept experiment for superplastic forming of complex shapes into dies [2].

Biaxial dome formation occurring by transformation superplasticity has been investigated only once before, by Dunand and Myojin [32], who observed greater strains after multiple thermal cycles in Ti-6Al-4V and Ti-6Al-4V/TiC_p composites (as compared to isothermal deformation). While it demonstrated that transformation superplasticity enhances deformation, their study did not present kinetic data describing the growth of domes under biaxial stress, or model the biaxial problem in the framework of Greenwood and Johnson's uniaxial model. The goal of the present study is to address these issues. Specifically, we investigate the kinetics of dome formation during gas pressure forming of Ti-6Al-4V and Ti-6Al-4V/TiC_p (the same materials used in Ref. [32]), as well as commercial purity titanium, Ti/TiC_p and Ti-6Al-4V/TiB_w. We also adapt an existing model of biaxial doming to include Greenwood and Johnson's constitutive law (Eq. (1)), and compare the predicted deformation kinetics with the experimental results.

Experimental Procedures

Experimental Materials

All materials were fabricated by Dynamet Technology (Burlington, MA) using their CHIP process [33, 34], which consists of blending of elemental metallic powders, cold isostatic pressing, vacuum sintering, and finally containerless hot isostatic pressing. The process was used to fabricate commercial-purity titanium (CP-Ti) and Ti-6Al-4V, with and without discontinuous reinforcements. Specifically, TiC particles in the amount of 10 vol.% were added to both CP-Ti and Ti-6Al-4V (these composites will be referred to simply as Ti/TiC_p and Ti-6Al-4V/TiC_p hereafter). Also, Ti-6Al-4V reinforced with 5 vol.% TiB whiskers (referred to as Ti-6Al-4V/TiB_w hereafter) was synthesized by including TiB_2 particulates during blending, which subsequently dissolved and reprecipitated as TiB whiskers during sintering and hot isostatic pressing [35-37].

Because the microstructures of the experimental materials have been extensively examined in the literature (e.g., in Refs. [22, 32-34]), they are only briefly described here. CP-Ti is single-phase, with large α-grains with an average diameter around 200 μm, while Ti-6Al-4V exhibits a microstructure common to two-phase $\alpha + \beta$ alloys, with α-phase laths about 80 μm in length, separated by β-phase, in the amount of about 10 vol.% at room temperature. Typical TiC particles (in either matrix) are about 20 μm in diameter, and are near equiaxed. Finally, the TiB whiskers are known to be randomly oriented (in composites with twice the volume fraction used in this work [25]), with a length greater than 30 μm and a diameter of about 5 μm.

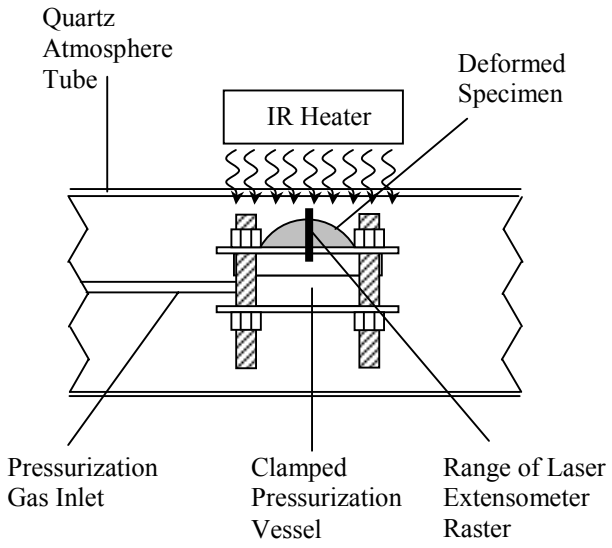

Figure 1. Schematic of the experimental biaxial gas-pressure apparatus, showing the central section of the quartz atmosphere tube, with a deformed specimen clamped in the pressurization vessel. The range of the laser raster is also shown.

Disks of each material were machined from near-net-shape densified plates, with density greater than 99%. The disks had a diameter of 62 mm and a thickness ranging from 1.36 to 1.59 mm (listed in Table I). Before testing, biaxial disk specimens were coated with Deltaglaze 153, a borosilicate glass paste from Acheson Colloids (Port Huron, MI), which forms a continuous coating upon exposure for 20 minutes at 950° C, thus preventing contamination with residual atmospheric gases and decreasing surface reflectivity (for more efficient radiative heating).

Biaxial Superplasticity Experiments

The apparatus for performing biaxial doming experiments is shown in Figure 1, and is described in greater detail in Ref. [38]. The disk specimens were clamped (using threaded Inconel rods and nuts) into an Inconel pressurization vessel with an open die radius of 24 mm. The specimen and pressurization vessel were placed in a quartz tube under a flowing inert argon atmosphere at ambient pressure, and heated by a radiant area heater with maximum power density of 32 W/cm^2 situated about 6 cm above, and parallel to, the specimen surface. Measurements of the dome height were taken without contacting the specimen, using a laser extensometer (from LaserMike, Dayton, OH) perpendicular to the quartz tube, as described in more detail later.

Specimens were heated to 840 °C in about 2 minutes and held at that temperature for 6-8 minutes. The specimen holder was then pressurized to 207 kPa (30 psi) above ambient pressure and the temperature cycling was initiated. The minimum temperature of each cycle was 840 °C, with a maximum temperature as indicated in Table I. Ti-matrix materials were thermally cycled at a frequency of 15 hr^{-1}, while Ti-6Al-4V matrix materials had a frequency of 7.5 hr^{-1}. Longer thermal cycles were performed for the Ti-6Al-4V-based materials due to the slower transformation kinetics [39]. Multiple cycles were performed for approximately 100 minutes, corresponding to 25 cycles for CP-Ti and Ti/TiC_p, and about 12 cycles for Ti-6Al-4V-based materials. The dome was then cooled for about 20 minutes, and its height was measured (with an accuracy of about 0.1 mm) with the laser extensometer at a temperature of about 150° C. This procedure was repeated several times for each specimen, giving a history of the dome height. After 3-5 sets of cycles, the specimen holder was removed from the quartz tube and a measurement of the dome height was taken with calipers to verify the laser measurements. Negligible discrepancies (at most 0.3 mm) were found. Experiments were terminated after times ranging from 15,840 s (for CP-Ti) to 54,720 s (for Ti-6Al-4V) with no dome rupture.

Each dome was sectioned along a diameter with a high-speed diamond blade, and digital images were taken of the resulting cross-section. The thickness distribution was found as a function of position along the dome by image analysis. An edge-finding algorithm was used to locate the upper and lower surface of the dome from which average thickness values were determined at equiangular steps of 0.02 radians along the dome profile. Thickness measurements equally distant from the dome apex and on opposite sides of the profile were averaged. Mirror symmetry was observed to within 60 μm indicating uniform deformation (unlike earlier experiments in Ref. [32], where the specimens were oriented vertically and slumped under the action gravity). On several specimens, a point micrometer was used to measure the thickness at various points on the dome surface. Within experimental accuracy, this procedure yielded identical measurements to those obtained through the image analysis procedure, validating the accuracy of this method.

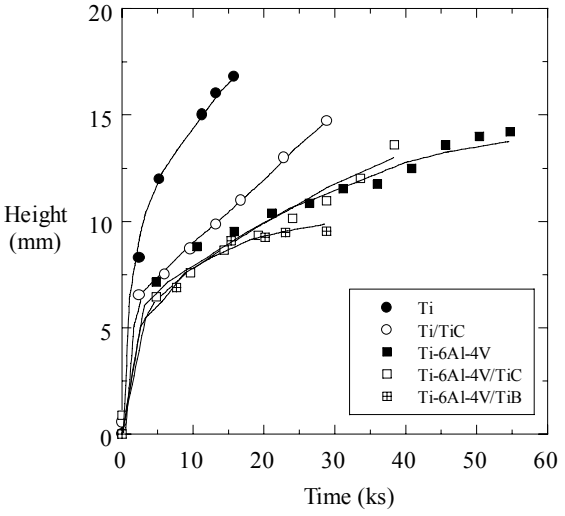

Figure 2. Dome height as a function of time for each material

Results

The dome height as measured by laser extensometer is shown as a function of time in Figure 2. The curves display the typical shapes of isothermal, constant-pressure biaxial doming experiments where fine-grain superplasticity is the active deformation mechanism [40-45]: the deformation, which is initially very rapid, becomes slower as the dome height increases. As expected, the weakest material, CP-Ti, deformed most rapidly, while the Ti-6Al-4V-based materials deformed more slowly due to the longer thermal cycle times and higher creep resistance. The thickness profiles for each specimen are displayed in Figure 3, in terms of relative thickness, s/s_o, where s is the final and s_o the initial thickness (given in Table I). The error bars correspond to the standard deviation over the averaging range of 0.02 radians. As expected, dome height (Fig. 2) is correlated with apex thickness reduction (Fig. 3): CP-Ti bulged most and is thinnest at the apex, while Ti-6Al-4V/TiB_w is the least bulged and thickest at the apex. Final apex thickness values are listed in Table I, together with von Mises equivalent strains (assuming equibiaxial strains at the apex). The most deformed CP-Ti sheet exhibits a true apex strain of 0.78, corresponding to an engineering strain of 119%.

Table I. Experimental materials and conditions

	Ti	Ti/TiC_P	Ti-6Al-4V	Ti-6Al-4V/TiC_P	Ti-6Al-4V/TiB_W
Max. cycle temp (°C)	965	970	970	970	980
Original Thickness (mm)	1.390	1.360	1.391	1.510	1.590
Final Thickness (mm)	0.636	0.759	0.878	1.179	1.372
Predicted Apex Thickness Eq. (19)	0.823	0.891	0.943	1.058	1.362
Predicted Apex Thickness Eq. (21)	0.628	0.715	0.772	0.868	1.210
Von Mises equivalent strain	0.78	0.58	0.46	0.25	0.15

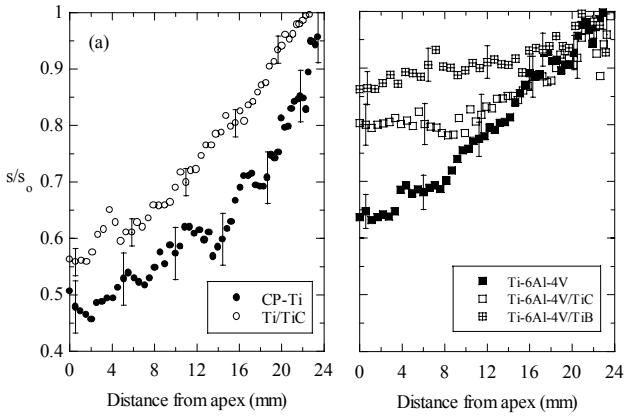

Figure 3. Thickness profile (normalized by original sheet thickness, s_o) for (a) CP-Ti and its composite and (b) Ti-6Al-4V and its composites

Discussion

Modeling Biaxial Deformation

The following discussion of biaxial doming uses the same assumptions used in the first detailed description of biaxial deformation by Jovane [40], i.e., isotropy, incompressibility, negligible bending effects, power-law deformation and a spherical geometry. However, we account for the variation in stress along the dome profile and for the non-uniform thickness distribution, as done by later authors [43, 44, 46]. In addition, we consider the operation of two deformation mechanisms (power-law creep and transformation superplasticity). Based on the developments of Enikeev and Kruglov [44], we also directly derive a compact differential equation for the rate of change in the dome height which can be numerically solved to determine the full height history of a bulging dome. The model presented below assumes that the dome is part of a sphere (i.e., a spherical cap) at all times during the experiments. By examining the dome profiles after deformation, we found that this condition was fulfilled for all specimens as described in Ref. [51].

For the doming geometry (Fig. 4), three principal stresses are the hoop stress, σ_h, the radial stress, σ_r, and the thickness stress, σ_s, described in an orthogonal, curvilinear coordinate system centered at the apex of the dome and fitted to the dome surface. Because of the traction-free surface condition on the upper side of the thin disk, the thickness stress is small enough that it may be neglected. The radial stress at any point within the dome with thickness, s, can be determined by thin shell theory as [40]:

$$\sigma_r = \frac{p \cdot R}{2 \cdot s} \tag{2}$$

where p is the gas pressure and R is the radius of curvature of the dome. Due to the geometric constraint at the dome edge, a plane-strain state exists in this region, with the hoop stress given as [43]:

$$\sigma_h = \frac{\sigma_r}{2} \tag{3}$$

and the radial (ε_r), thickness (ε_s) and hoop (ε_h) strains as [47]:

$$\varepsilon_r = -\varepsilon_s \tag{4a}$$
$$\varepsilon_h = 0 \tag{4b}$$

However, at the apex, the stress state is balanced biaxial [40]:

$$\sigma_h = \sigma_r \tag{5}$$
$$\varepsilon_r = \varepsilon_h = -2\varepsilon_s \tag{6}$$

The von Mises equivalent stress σ_{eq} and strain rate $\dot{\varepsilon}_{eq}$ at the apex may thus be found as:

$$\sigma_{eq} = \sigma_r \tag{7a}$$
$$\dot{\varepsilon}_{eq} = -\dot{\varepsilon}_s \tag{7b}$$

Based on the deformation of a half-meridian, the thickness at the apex s_a has been derived by Enikeev and Kruglov [44] as:

$$s_a = s_o \cdot \left(\frac{\sin\alpha}{\alpha}\right)^2 \tag{8}$$

where s_o is the uniform thickness of the undeformed sheet and α is the angle subtended by the apex and the edge of the dome (Fig. 4).

The effective strain rate at the apex was given in Eq. (7) as being equal in magnitude to the thickness strain rate, $\dot{\varepsilon}_s$, which is defined as:

$$\dot{\varepsilon}_s = \frac{\dot{s}_a}{s_a} \tag{9}$$

Using Eqs. (8,9), the thickness strain rate at the apex can be found as:

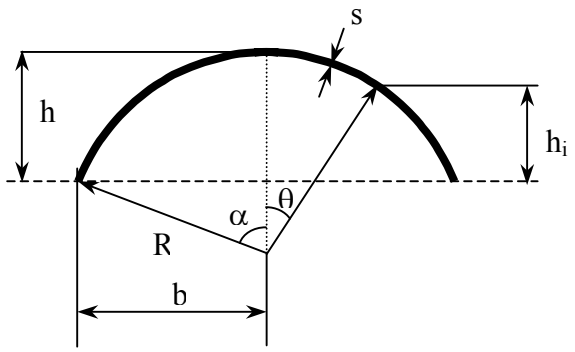

Figure 4. Schematic of dome geometry used in modeling

$$\dot{\varepsilon}_s = -2\dot{\alpha} \cdot \left(\frac{1}{\alpha} - \cot\alpha \right) \quad (10)$$

A simplified uniaxial constitutive law which can describe many different deformation mechanisms is:

$$\dot{\varepsilon} = K \cdot \sigma^n \quad (11)$$

where K is a temperature-dependent parameter. For transformation superplasticity, the stress exponent, n, has a value of unity at low stresses (Eq.(1)). However, during a thermal cycle, transformation superplasticity contributes to the deformation only when the phase transformation is occurring. At all other times, the material deforms only under the action of the external stress by a typical creep mechanism (e.g., dislocation creep). Since these two mechanisms operate at different times during the cycle, they contribute to the total deformation independently, and it is reasonable to add their contributions [48]:

$$\dot{\varepsilon} = \dot{\varepsilon}_{creep} + \dot{\varepsilon}_{TSP} = K_{creep} \cdot \sigma^n + K_{TSP} \cdot \sigma \quad (12)$$

Eq. (12) is a simple constitutive creep law valid only for the uniaxial case. To find the thickness strain rate, a more generalized equation involving the multiaxial stress state is required [49]:

$$\dot{\varepsilon}_1 = K_{creep} \cdot \sigma_{eq}^{n-1} \cdot \left[\sigma_1 - \frac{1}{2}(\sigma_2 + \sigma_3) \right] + K_{TSP} \cdot \left[\sigma_1 - \frac{1}{2}(\sigma_2 + \sigma_3) \right] \quad (13)$$

where 1, 2, and 3 are the principle directions. Upon introduction of Eqs. (2) and (7) into Eq. (13), the thickness strain rate at the apex is found as:

$$-\dot{\varepsilon}_s = K_{creep} \cdot \sigma_r^n + K_{TSP} \cdot \sigma_r \quad (14)$$

Combining Eqs. (2), (10) and (14) then results in:

$$K_{creep} \cdot \left(\frac{pR}{2s_a} \right)^n + K_{TSP} \cdot \frac{pR}{2s_a} = 2\dot{\alpha} \cdot \left(\frac{1}{\alpha} - \cot\alpha \right) \quad (15)$$

The above equation is equivalent to Eq. (7) in Ref. [44], for the case of a single deformation mechanism (i.e., K_{TSP} = 0). Substituting Eq. (8) and noting that R = b/sinα (Fig. 4), Eq. (15) becomes:

$$K_{creep} \cdot \left(\frac{pb}{2s_o} \frac{\alpha^2}{\sin^3\alpha} \right)^n + K_{TSP} \cdot \frac{pb}{2s_o} \frac{\alpha^2}{\sin^3\alpha} = 2\dot{\alpha} \cdot \left(\frac{1}{\alpha} - \cot\alpha \right) \quad (16)$$

Defining the non-dimensional apex height, η = h/b, which is equal to zero when the disk is flat and unity at a hemisphere, and noting that η = tan(α/2) from geometry, Eq. (16) can be rewritten as:

$$\dot{\eta} = \frac{1}{2} \cdot \frac{\eta \cdot \arctan\eta \cdot (1+\eta^2)}{\eta - \arctan\eta \cdot (1-\eta^2)} \cdot \left[K_{creep} \cdot S^n + K_{TSP} \cdot S \right] \quad (17)$$

where

$$S = \frac{pb}{4s_o} \cdot \frac{\arctan^2\eta \cdot \left(1+\eta^2\right)^3}{\eta^3} \quad (18)$$

Eq. (17) thus presents a simple differential equation for the rate of change in the dome height, as a function of the temperature, forming pressure, instantaneous height, initial sheet thickness and radius, and known materials parameters. In the sections to follow, we numerically evaluate Eq. (17) to predict the apex height history during thermal cycling experiments, first for the unreinforced materials, and later for the metal matrix composites.

Biaxial Deformation of CP-Ti and Ti-6Al-4V

We first discuss the model predictions for CP-Ti and Ti-6Al-4V, as the values of the pre-stress deformation constants, K_{TSP} and K_{creep}, are well characterized by uniaxial experiments, and the model can thus be implemented without the use of any adjustable parameters.

In the case of CP-Ti, we consider the contributions from both creep and transformation superplasticity. For the latter mechanism, the superplastic slope, $d\Delta\varepsilon/d\sigma = 2.3\ GPa^{-1}$ has been determined from several studies [11, 23, 24] with different cycle amplitudes and frequencies, after accounting for extraneous creep contributions to the total deformation. The pre-stress constant $K_{TSP} = \nu \cdot d\Delta\varepsilon/d\sigma$ is then found as $9.58 \times 10^{-12}\ Pa^{-1} \cdot s^{-1}$. The contribution of creep during a thermal cycle is found by integrating the dislocation creep rate over the portions of the thermal cycle above the β-transus (found at 955° C) and neglecting creep in the more creep resistant α-phase, as discussed in Refs. [22, 23]. The creep law of β-Ti in Ref. [50], with a power-law stress exponent of n = 4.3, was used. By numerically averaging over the experimentally measured thermal cycles, the effective, average value of K_{creep} during the biaxial doming experiments is found as $5.0 \times 10^{-34}\ Pa^{-4.3} \cdot s^{-1}$.

The model predictions for biaxial doming of CP-Ti are compared with the experimental results in Figure 5, and the agreement is very good, especially considering that no adjustable parameters were used. Also shown are the individual contributions of transformation superplasticity and dislocation creep of β-Ti, found by setting K_{creep} and K_{TSP}, respectively, to zero in Eq. (17). Clearly the biaxial deformation is primarily due to transformation superplasticity, with a small but non-negligible contribution from creep. It should also be noted that the individual contributions to dome height shown in Figure 5 are not additive; rather, the rates of dome growth are additive according to Eq. (17).

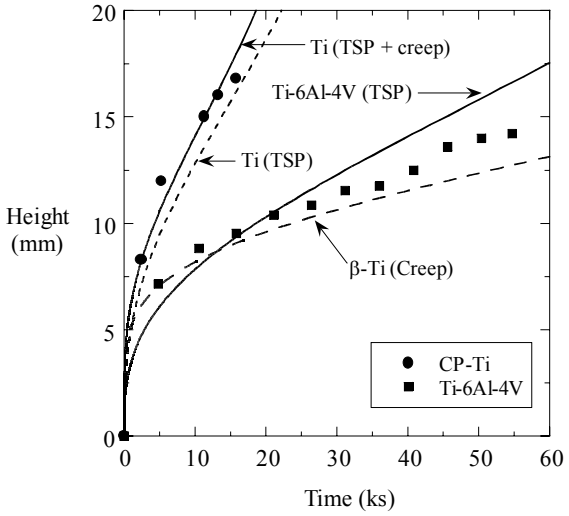

Figure 5. Experimental time-dependence of dome heights for CP-Ti and Ti-6Al-4V. Model predictions (Eq. (17)) are shown for all active deformation mechanisms.

For the case of Ti-6Al-4V, the experimental thermal cycles did not cross the β-transus at 1000 °C [39], so the material was in the process of transforming at all times during the cycle [4]. Thus, all of the measured deformation can be attributed to transformation superplasticity, and no contribution from creep need be added to the model (K_{creep} = 0). For 8-minute cycles between 840-970 °C, Ref. [4] gives the superplastic slope, $d\Delta\varepsilon/d\sigma$ = 1.25 GPa^{-1}, from which K_{TSP} is found as $\nu \cdot d\Delta\varepsilon/d\sigma = 2.6 \times 10^{-12}$ $Pa^{-1} \cdot s^{-1}$. The predictions of the model are compared to the experimental results in Figure 5 and, as for CP-Ti, the agreement is good.

Biaxial Deformation of Composite Materials

In contrast to the unreinforced materials, creep and transformation superplasticity characteristics of the composite materials are less thoroughly characterized in uniaxial tension, and the existing studies use different thermal cycles profiles and/or different volume fractions of reinforcement. Therefore, in this section, we consider K_{TSP} as an adjustable parameter, fit solutions of Eq. (17) to the experimental data, and compare the fitted values of K_{TSP} to those reported previously in the literature. As already discussed for unreinforced Ti-6Al-4V, transformation superplasticity is the only operative deformation mechanism for the Ti-6Al-4V composites, and there is no contribution from creep. Also, as described in literature for Ti/TiC_p, the presence of dissolved carbon and oxygen in the CP-Ti matrix increases the β-transus temperature (to about 995 °C), eliminating any excursion into the β-field during the biaxial experiments, for which the maximum cycle temperature was 970 °C [23, 24]. Thus, for all of the composite materials, the contribution of creep outside the transformation temperature range is assumed to be negligible (K_{creep} = 0).

In Figure 6a-c, we show the experimental data and model predictions for Ti/TiC_p, $Ti\text{-}6Al\text{-}4V/TiC_p$, and $Ti\text{-}6Al\text{-}4V/TiB_w$, respectively, using three different values of K_{TSP} for each material. The value of K_{TSP} which best describes the experimental results is listed in Table II, along with values from several literature studies on similar materials. For both Ti-6Al-4V composites, the agreement between the fitted values of K_{TSP} and the values from the literature on uniaxial experiments is satisfactory (within a factor of 1.4). For both materials, the disagreement is most likely due to the lower cycle amplitudes used in the present study (Table I) as compared to literature studies, eliminating the creep contribution to deformation and limiting the extent of the phase transformation. For the case of $Ti\text{-}6Al\text{-}4V/TiB_w$, whisker alignment during deformation may also reduce the observed value of K_{TSP} due to strain hardening [25].

A larger disagreement on the value of K_{TSP} was observed for Ti/TiC_p (Table II). The slower-than-expected bulging is perhaps caused by an incomplete transformation, as discussed above and in Refs. [23, 24]. In other uniaxial studies [22-24], wide variation in K_{TSP} values has been reported for Ti/TiC_p (see Table II), such that the observed variation is still reasonable. Again, the cycle amplitude for the biaxial experiments was somewhat lower than for the uniaxial experiments from which literature values were taken.

Table II. Comparison of fitted biaxial, experimental uniaxial, and literature values for the transformation superplasticity constants K_{TSP} and $d\Delta\varepsilon/d\sigma$.

	Experimental	Literature Values	
	K_{TSP} Biaxial (10^{12} $Pa^{-1} \cdot s^{-1}$)	K_{TSP} Uniaxial (10^{12} $Pa^{-1} \cdot s^{-1}$)	Reference
Ti/TiC_P	4.2	5.0-13.3	[22-24]
$Ti\text{-}6Al\text{-}4V/TiC_P$	2.5	2.3-3.5	[24, 51, 52]
$Ti\text{-}6Al\text{-}4V/TiB_W$	2.4	2.9	[51]

The above results show that transformation superplasticity can fully account for the measured deformations in all three composites. In what follows, we compare the measured values to upper-bound predictions for deformation by creep alone, in the absence of an enhancement due to the phase transformation. For this purpose, the creep rate of the matrix material (CP-Ti or Ti-6Al-4V) is taken as an upper-bound of the creep rate of the respective composite materials, since isothermal creep of the composites is slower than for the unreinforced matrices [22, 24, 53, 54]. For the case of Ti-6Al-4V, the average creep rate during cycling (in the absence of transformation superplasticity) is found by averaging experimental isothermal creep data [55] over the temperature range of the thermal cycle (840 – 970 °C). As discussed above, it is likely that the matrix of the Ti/TiC_p composite did not fully transform during the present thermal cycles; thus the creep of α-Ti [50] is considered for comparison with the Ti/TiC_p composites. As before, the expected creep rate during cycling (without transformation) is found by numerical averaging of this creep rate over the thermal cycle.

The amount of dome growth expected by creep during thermal cycling, if there were no enhancement due to the phase transformation, is shown as a dashed line in Figs. 6a-c. When

compared with these trendlines, the experimental data clearly verify that transformation superplasticity is active during thermal cycling, as creep alone could not result in such large deformation for any of these composites. Although we did not achieve superplastic strains in all of the materials (i.e., engineering thickness strain of 120% for CP-Ti and less than 80% for all other materials), the operation of the transformation superplasticity deformation mechanism is further confirmed by this analysis. Thus, if longer experimental times or larger forming pressure were used, superplastic strains (>100%) could be achieved, as shown in Ref.[32], for Ti-6Al-4V and Ti-6Al-4V/TiC_p domes.

Thickness Modeling

In this section, two existing models are presented for predicting the final thickness distribution in the domes. The first was developed by Enikeev and Kruglov [44], who make the assumption that each meridian passing through the dome apex is uniformly deformed at any point in time. The model also assumes an appropriate variation in stress state from balanced biaxial at the apex to plane-strain at the periphery. The authors develop the following equation for the variation in the thickness, s, as a function of position in the dome:

$$s = s_o \cdot \left(\frac{\sin\alpha}{\alpha} \right)^2 \cdot \frac{\theta}{\sin\theta} \tag{19}$$

where the angle θ is illustrated in Fig. 6. At $\theta = 0$, this expression reduces to Eq. (8), giving the thickness, s_a, at the dome apex, while at $\theta = \alpha$ at the dome periphery, the thickness is reduced by a factor of $\alpha/\sin\alpha$ (i.e., $s/s_o = \sin\alpha/\alpha$).

The second thickness distribution model is that of Ragab [41], which like that of Enikeev and Kruglov [44], is based solely on geometry. However it assumes a balanced biaxial stress state throughout the dome. The thickness at any point is given as:

$$s = s_o \cdot \left(1 + \frac{h_i \cdot h}{b^2} \right)^{-2} \tag{20}$$

where h_i is the local height of the dome at any radial position. By substituting for h_i, h and b in terms of α and θ (Fig. 4), Eq. (20) becomes:

$$s = s_o \cdot \left(\frac{\cos\alpha + 1}{\cos\theta + 1} \right)^2 \tag{21}$$

At the periphery of the dome ($\theta = \alpha$), Ragab's model [41] (Eq. (21)) predicts no reduction in thickness ($s_a = s_o$), unlike the model of Enikeev and Kruglov [44] (Eq. (19)).

A comparison of measured apex thickness values and theoretical thickness predictions for each model (Eqs.(19) and (21)), and for each material, is presented in Table I. Both models are reasonably accurate at the apex, except in the case of Ti-6Al-4V/TiC_p. Although we presently compare these models only to

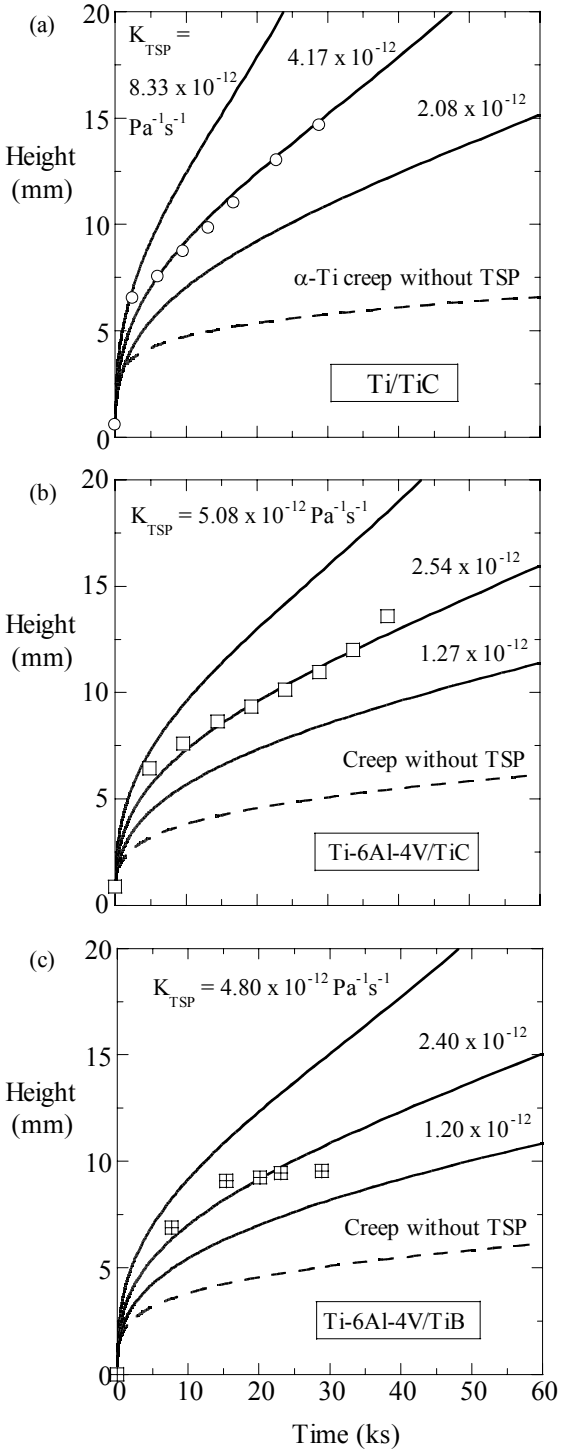

Figure 6. Comparison of experimental results and model predictions with different values of K_{TSP} as a fitting parameter for (a) Ti/TiC_p, (b) Ti-6Al-4V/TiC_p, and (c) Ti-6Al-4V/TiB_w. Also shown is the expected amount of creep deformation during thermal cycling (dashed lines), in the absence of any transformation superplasticity contribution.

the apex thickness, a detailed comparison at all radial positions is possible, as described in more detail in Ref. [51].

Conclusions

The present study has investigated biaxial deformation by transformation superplasticity in unalloyed titanium (CP-Ti), a titanium alloy (Ti-6Al-4V), and three titanium matrix composites (Ti/10 vol.% TiC_p, Ti-6Al-4V/10 vol.% TiC_p, Ti-6Al-4V/5 vol.% TiB_w). Thermal cycling experiments were performed while simultaneously subjecting specimens to an external stress, i.e., biaxial gas pressurization of a sheet specimen. The major results are summarized below.

- Biaxial deformation of titanium alloys and composites is enhanced by thermal cycling as compared to isothermal deformation. Local strains were determined by image analysis of deformed dome sections, and the maximum engineering strain observed was 119% for CP-Ti. For three of the experimental materials (CP-Ti, Ti/TiC_p and Ti-6Al-4V/TiB_w), these experiments constituted the first demonstration of biaxial transformation superplasticity.
- Analytical predictions based on the model of Enikeev and Kruglov [44] accurately predicts the dome height kinetics and the measured thickness distributions of the deformed specimens. The kinetic model also revealed the relative contributions of transformation superplasticity and creep during biaxial deformation, and showed that deformation by isothermal creep alone would results in significantly longer times to attain the same degree of deformation as thermal cycling.

Acknowledgements

This work was funded by NSF SBIR #9901850, through a subcontract from Dynamet Technology, Burlington, MA, and the US DoD, through a graduate fellowship for C.S., who also acknowledges partial support from the U.S. Department of Energy, through the University of California, Lawrence Livermore National Laboratory under contract No. W-7405-Eng-48

References

1. S. Lampman, *Wrought Titanium and Titanium Alloys*, in *ASM Handbook: Properties and Selection: Nonferrous Alloys and Special Purpose Materials*, ASM International, Metals Park, OH, (1990)
2. T. G. Nieh, J. Wadsworth and O. D. Sherby, *Superplasticity in Metals and Ceramics,* Cambridge University Press, Cambridge (1997)
3. G. W. Greenwood and R. H. Johnson, *Proc. Roy. Soc. Lond.,* 283, 403-422 (1965)
4. C. Schuh and D. C. Dunand, *Acta Mater.,* 49, 199-210 (2001)
5. F. W. Clinard and O. D. Sherby, *Acta Metall.,* 12, 911-919 (1964)
6. A. G. Young, K. M. Gardiner and W. B. Rotsey, *J. Nucl. Mat.,* 2, 234 (1960)
7. D. Oelschlagel and V. Weiss, *Trans. Quart. ASM,* 59, 143-154 (1966)
8. T. B. Massalski, S. K. Bhattacharyya and J. H. Perepezko, *Metall. Trans.,* 9A, 53-56 (1978)
9. M. deJong and G. W. Rathenau, *Acta Metall.,* 7, 246-253 (1959)
10. M. deJong and G. W. Rathenau, *Acta Metall.,* 9, 714-720 (1961)
11. R. Kot, G. Krause and V. Weiss, *Transformation Plasticity of Titanium*, in *The Science, Technology and Applications of Titanium*, Pergamon, Oxford, (1970)
12. C. Chaix and A. Lasalmonie, *Res Mechanica,* 2, 241 (1981)
13. M. Lozinsky, *Acta Metall.,* 9, 689 (1961)
14. K. Sato, T. Nishimura and Y. Kimura, *Materials Science Forum,* 170-172, 207 (1994)
15. P. Zwigl and D. C. Dunand, *Metall. Mater. Trans.,* 29A, 2571-2582 (1998)
16. K. Nuttall and D. P. McCooeye, *Phase Transformation Plasticity in Zirconium-Hydrogen Alloys*, in *Mechanical Behavior of Materials*, The Society of Materials Science, Japan, (1974)
17. K. Nuttall, *Scripta Met.,* 10, 835-840 (1976)
18. M. Zamora and J. P. Poirier, *Mechanics of Materials,* 2, 193-202 (1983)
19. R. H. Johnson and G. W. Greenwood, *Nature,* 195, 138-139 (1962)
20. G. W. Greenwood and R. H. Johnson, *React. Sci. Technol.,* 16, 473 (1962)
21. C. Schuh and D. C. Dunand, *Acta Mater.,* 46, 5663-5675 (1998)
22. D. C. Dunand and C. M. Bedell, *Acta Mater.,* 44, 1063 (1996)
23. C. Schuh and D. C. Dunand, *Scripta Mater.,* 40, 1305-1312 (1999)
24. C. Schuh, W. Zimmer and D. C. Dunand, Creep Behavior of Advanced Materials for the 21st Century, The Minerals, Metals & Materials Society, 61-70 (1999)
25. C. Schuh and D. C. Dunand, *International Journal of Plasticity,* 17, 317-340 (2001)
26. C. A. Johnson, R. C. Bradt and J. H. Hoke, *J. Am. Ceram. Soc.,* 58, 37-40 (1975)
27. D. C. Dunand and J. L. Grabowski, *J. Am. Ceram. Soc.,* 83, 2521-2528 (2000)
28. O. A. Ruano, J. Wadsworth and O. D. Sherby, *Metall. Trans.,* 13A, 355-361 (1982)
29. C. Schuh, P. Noël and D. C. Dunand, *Acta Mater.,* 48, 1639-1653 (2000)
30. D. C. Dunand and J. Teisen, in *Porous and Cellular Materials for Structural Applications, MRS Proceedings,* 521, 231-236 (1998)
31. N. G. Davis, J. Teisen, C. Schuh and D. C. Dunand, *Journal of Materials Research,* 16, 1508-1519, (2001)
32. D. C. Dunand and S. Myojin, *Mater. Sci. Eng.,* A230, 25-32 (1997)
33. S. Abkowitz and P. Weihrauch, *Advanced Materials and Processes,* 7, 31-34 (1989)
34. S. Abkowitz, P. F. Weihrauch and S. M. Abkowitz, *Industrial Heating,* 12, 32-36 (1993)

35. M. E. Hyman, C. McCullough, J. J. Valenci, C. G. Levi and R. Mehrabian, *Metall. Trans.,* 20A, 1847-1859 (1989)
36. T. Saito, *Advanced Performance Materials,* 2, 121-144 (1995)
37. K. Funami, M. Kobayashi, S. Suzuki and C. Ouchi, *Materials Science Forum,* 243-245, 515-520 (1997)
38. M. Frary, *Biaxial Transformation Superplasticity of Titanium Alloys and Composites*, M.S. Thesis, Northwestern University, Evanston, IL, (2001)
39. W. Szkliniarz and G. Smolka, *Journal of Materials Processing Technology,* 53, 413-422 (1995)
40. F. Jovane, *Int. J. Mech. Sci.,* 10, 403-427 (1968)
41. A. R. Ragab, *Metals Technology,* 10, 340-348 (1983)
42. S. Yu-Quan and Z. Jun, *Mater. Sci. Eng.,* 84, 111-125 (1986)
43. Z. X. Guo and N. Ridley, *Mater. Sci. Eng.,* A114, 97-104 (1989)
44. F. U. Enikeev and A. A. Kruglov, *Int. J. Mech. Sci.,* 37, 473-483 (1995)
45. C. F. Yang, L. H. Chiu and S. C. Lee, *Scripta Mater.,* 34, 1555-1560 (1996)
46. A. K. Ghosh and C. H. Hamilton, *Metall. Trans.,* 13A, 733-743 (1982)
47. A. Dutta and A. K. Mukherjee, *Mater. Sci. Eng.,* A157, 9-13 (1992)
48. T. H. Courtney, *Mechanical Behavior of Materials,*McGraw-Hill, Inc., New York (1990)
49. I. Finnie and W. R. Heller, *Creep of Engineering Materials,*McGraw-Hill Book Company, Inc., New York (1959)
50. H. J. Frost and M. F. Ashby, *Deformation Mechanism Maps,*Pergamon Press, Oxford (1982)
51. M. Frary, C. Schuh and D. C. Dunand, *Metall. Mater. Trans.,* in print, (2001)
52. C. Schuh and D. C. Dunand, *Materials Science Forum,* 357-359, 177-182 (2001)
53. S. Ranganath and R. S. Mishra, *Acta Mater.,* 44, 927-935 (1996)
54. S. J. Zhu, Y. X. Lu, Z. G. Wang and J. Bi, *Material Letters,* 13, 199-203 (1992)
55. C. Schuh and D. C. Dunand, *Journal of Materials Research,* 16, 865-875 (2001)